Principal Modes of Southern Hemisphere Low-Frequency Variability Obtained from NCEP–NCAR Reanalyses

JOHN W. KIDSON

National Institute of Water and Atmospheric Research Ltd., Wellington, New Zealand

(Manuscript received 30 April 1998, in final form 8 December 1998)

ABSTRACT

Analysis of the 300-hPa streamfunction from the 40-year NCEP–NCAR dataset has identified the principal modes of Southern Hemisphere variability on intraseasonal (IS), interannual (IA), and intradecadal (ID) timescales. The variance of streamfunction departures from the annual cycle is zonally symmetric in the IS and IA range with the largest values at midlatitudes. The ID variance is concentrated in the Pacific sector, where it extends to lower latitudes.

For the IS band, obtained by applying a 10–50-day bandpass filter to the twice-daily streamfunction fields, three pairs of EOF patterns were obtained. These show eastward-propagating wavenumber-4 and -5 patterns largely confined to middle and higher latitudes, and two interleaved wavenumber-4 patterns expressing intensification of the zonal wind near 30°S. The wavenumber-5 patterns are more prominent in summer (December–February).

On the interannual timescale, including all periods beyond 50 days, the leading EOF with 26% of the variance expresses fluctuations in the strength of the subtropical jet. EOFs 2 and 3 contain mixed representations of the high-latitude mode and an ENSO (El Niño–Southern Oscillation) related pattern largely confined to the Pacific. EOFs 4 and 5 depict a wave train extending from Australia across the South Pacific to the east of South America. These appear to be stable throughout the period of analysis and contribute around 52% of the >50-day variance.

Variations on ID timescales were isolated by forming 11-month running means of the streamfunction anomalies, and five leading EOFs were found to be significant. The first of these, with 37% of the variance, captured variations forced by ENSO that extend from the equator to higher latitudes in the South Pacific. The second EOF with 18% of the variance accounted for changes in the circulation occurring in the early part of the record, and its amplitude since 1970 has been small. The third was identifiable as the high-latitude mode.

1. Introduction

Over the last two decades many investigators have examined aspects of low-frequency variability of the Southern Hemisphere (SH) circulation, on both interannual and intraseasonal timescales. Most have concentrated on middle and high latitudes where the variance in the geopotential height field is greatest (e.g., Trenberth 1981). A number of the earlier studies used archives of daily analyses from the World Meteorological Centre in Melbourne while, more recently, those from the European Centre for Medium-Range Weather Forecasts (ECMWF) have been favored. A detailed review of this earlier work has recently been presented by Kiladis and Mo (1998).

On the intraseasonal (IS) timescale, which typically covers periods in the range 10–50 days, the preferred modes of variation are stationary or eastward-propagating wave trains confined to the belt between 40° and 60°S, where the polar jet acts as a waveguide (Berbery et al. 1992; Ambrizzi et al. 1995). Wavenumbers 3 and 4 are most prominent in winter, but wavenumber 5 may be dominant for extended periods during the summer months. The patterns are nearly equivalent barotropic but tilt slightly westward with height (see Farrara et al. 1989; Ghil and Mo 1991; Kidson 1991; Mechoso et al 1991; Lau et al. 1994; Kiladis and Mo 1998). The tropical Madden–Julian oscillation (MJO) with periods in the 30–60 day range (e.g., Madden and Julian 1994) contributes to the variance in this frequency band and appears to be linked through tropical convection in the Australian sector to a wave train extending across the South Pacific to South America (Berbery and Nogues-Paegle 1993; Mo and Higgins 1998). Kiladis and Weickmann (1992a,b; 1997) have found more generally that IS teleconnection patterns may be forced by convection in the Indian and Australasian sectors.

The patterns of interannual (IA) variability at periods greater than 50 days show little variation with season (Rogers and van Loon 1982; Kidson 1988b). One of the main features to emerge from empirical orthogonal

Corresponding author address: Dr. John W. Kidson, NIWA, P.O. Box 14901, Wellington, New Zealand.
E-mail: j.kidson@niwa.cri.nz

function (EOF) analysis is the high-latitude mode (HLM) (e.g., Karoly 1990; Mo and White 1985; Mo 1986; Mo and Ghil 1987; Kidson 1988b; Kousky and Bell 1992; Kidson and Sinclair 1995). This has a high degree of zonal symmetry, expressing opposing variations in surface pressure fields across 55°–60°S and in the zonal winds near 40° and 60°S throughout the depth of the troposphere. Another consistent feature to emerge from the above studies is a wave train that extends southeastward from its source region in the vicinity of Australia across the South Pacific before recurving equatorward over South America. EOF analysis typically identifies it as two interleaved patterns with similar eigenvalues (e.g., Kidson 1988b; Kiladis and Mo 1998). The eastward end of this wave train was identified in the work of Mo and Ghil (1987), who called it the Pacific–South American (PSA) pattern by analogy with the three centers of the Pacific–North American pattern over North America (Wallace and Gutzler 1981). It will be referred to throughout this paper as the South Pacific wave train (SPW). Other patterns to emerge from the studies cited above include wavenumber 3 and 4 patterns extending around the polar vortex.

Of necessity, previous studies of IA and IS variability have been based on datasets for limited periods, typically 10–15 years. This has made it difficult to isolate seasonal variations in the patterns of low-frequency variance, to assess the stability of these patterns, and to identify changes occurring on the decadal timescale. A number of indices of the SH circulation show secular changes dating from the 1970s [see van Loon et al. (1993) and Renwick et al. (1998) for those occurring in the Australia–New Zealand sector]. These include a trend to more frequent negative incursions of the Southern Oscillation index and the virtual disappearance of the semiannual oscillation. It is of interest to see whether there may have been concomitant changes in the SH teleconnection patterns.

Another feature linking many of these earlier studies is their concentration on the variance of the geopotential height field, which tends to confine the teleconnection patterns to middle and higher latitudes. There are some exceptions, for example, Mo and Ghil (1987), who analyzed zonally filtered and normalized height anomalies, and the comparison of the leading EOFs obtained by the use of covariance and correlation matrices of the 500-hPa height field by Kidson (1988b). In order assess the importance of links between the Tropics and the circulation at higher latitudes, we need to employ analysis techniques that will give comparable weight to circulation changes in both regions. One such technique is the use of the streamfunction (Lau et al. 1994) that gives the same weight to perturbations in the wind velocity, vorticity, and kinetic energy at each latitude.

The new 40-year Reanalysis dataset from the National Centers for Environmental Prediction–National Center for Atmospheric Research (NCEP–NCAR) (Kalnay et al. 1996), while not without its problems, provides an excellent opportunity to address some of the shortcomings outlined above. This paper analyzes low-pass- and bandpass filtered twice-daily streamfunction values at 300 hPa, to examine the variability on IS and IA timescales. Monthly means of the streamfunction anomalies are also filtered to separate out intradecadal (ID) timescales, and empirical orthogonal function analysis has been employed in each case to identify the leading modes. While many of the observed patterns are likely to be linked to changes in the tropical circulation (e.g., Trenberth et al. 1998), analysis of these relationships is beyond the scope of the present paper.

2. Data and processing techniques

This analysis has been based on the NCEP–NCAR dataset comprising 12-h analyses at 2.5° spatial resolution between January 1958 and June 1997 (Kalnay et al. 1996). While this dataset is homogeneous, in that the same processing and analysis techniques have been used throughout, new types of observational data including satellite soundings, cloud motion vectors, and drifting buoys, have been added over the years, giving better coverage of oceanic regions. Prior to the First Global Atmospheric Research Program (GARP) Global Experiment (FGGE) year in 1979, coverage of the Southern Hemisphere was similar to that in the Newell et al. (1972) atlas with large gaps over oceanic areas. The NCEP–NCAR analyses will be better than in this early climatology, however, because the assimilation has been based on daily data rather than monthly mean land station values, allowing some propagation of features observed over land into oceanic areas and the incorporation of ship and aircraft observations.

Early attempts by the Australian Bureau of Meteorology to improve analysis over data-sparse areas through the interpretation of satellite imagery led to a large set of pseudo-observations (PAOB) that have unfortunately been included at incorrect positions between 1979 and 1992. It has not been feasible to repeat the assimilation for this period, but a comparison of the analyses with and without the faulty PAOB locations has been undertaken at the NOAA Climate Prediction Center.[1] This indicates that

- the SH middle and high latitudes (poleward of 40°S) are most affected by this error, particularly in winter;
- the largest differences are close to the surface and decrease rapidly with height; and
- the differences decrease rapidly as the timescale increases from synoptic to monthly and as the spatial scale increases.

[1] See http://wesley.wwb.noaa.gov/paobs/paobs_1.html for further information on the PAOB problem, and http://wesley.wwb.noaa.gov/ncep_data/index_wesley.html for monthly maps of data coverage.

Since this analysis uses data from the 300-hPa level with variability on the synoptic timescale removed by filtering, it is unlikely to be significantly affected.

As noted earlier, the low-frequency variations in the SH circulation are generally equivalent barotropic, showing similar anomaly patterns at all levels. The choice of a single level therefore provides an acceptable description of spatial teleconnection patterns, and the results should not depend greatly on the level chosen. With the increasing interest in linkages between the tropical and midlatitude circulation, an upper-tropospheric level was favored because it relates more directly to vorticity sources in the divergent flow. The 300-hPa level has been preferred here over the 200-hPa level used in some previous studies because it remains in the upper troposphere at all latitudes. There is little slope in isentropic surfaces at this level between the subtropics and the pole (e.g., Hoskins et al. 1989), and wave motion will be quasi-two-dimensional in the absence of diabatic effects.

In contrast to most previous studies, the analysis was performed on the streamfunction, which gives equal weight to velocity perturbations in the Tropics and at higher latitudes. This is preferable to using normalized variations in the geopotential height field as the geostrophic relationship breaks down in the Tropics and the interpretation of the results is unsatisfactory. The area of analysis was confined to the Southern Hemisphere in order to concentrate on patterns of variation within this region. The results of Lau et al.'s (1994) global EOF analysis did not produce good depictions of some patterns that are known from previous SH analyses and from some of those obtained here (such as the high-latitude mode and the high-latitude extension of the ENSO pattern). The need to derive coherent patterns associated with a common tropical source is likely to result in distortion of the patterns in each hemisphere while, as Lau et al. acknowledge, patterns of regional interest are likely to be omitted from a global analysis. The relatively small streamfunction variance along the equator (σ around $2 \times 10\ m^2\ s^{-1}$ compared to 5–7 ($\times 10\ m^2\ s^{-1}$) over the extratropics) also provides some support for confining the analysis to the SH.

The streamfunction was computed for each twice-daily analysis over the entire globe using routines, based on fast Fourier transforms, which were originally developed at ECMWF. Prior to EOF analysis a subset of points was extracted at 5° resolution in latitude and a variable resolution in longitude in order to provide a more even density of points and to avoid biasing the analysis toward high-latitude patterns. The east–west spacing between points was 5° longitude from the equator to 45°S, 10° between 50° and 65°S, 20° at 70° and 75°S, 40° at 80° and 85°S, and a single point at the pole, giving a total of 919 points.

In order to separate out intraseasonal and interannual variability, 10–50-day bandpass and 50-day low-pass filters were applied to the 12-hourly streamfunction fields. The filters are similar to those used by Kidson (1988b, 1991) and employ 23 and 36 weights, respectively, to give a reasonably sharp delineation of the spectral bands. This filtering also attenuates the errors in the analysis from the PAOB assimilation. The smoothed annual cycle was subsequently removed from the low-pass filtered data.

EOF analysis was performed on the filtered series, and the significant EOFs were selected for further study with the aid of the scree test (Craddock and Flood 1969). In each case the covariance matrix was computed from the order of 28 000 12-hourly observations. Given that independent data points are up to 10 days apart in SH midlatitudes, where most of the streamfunction variance is observed (see Kiladis and Mo 1998), the North et al. (1982) criterion for degeneracy is uncertainty of $(2/1400)^{1/2}$ or $\pm 3.8\%$ in the eigenvalues. Successive EOFs for which the ratio of the eigenvalues is ≤ 1.08 are therefore likely to have mixed spatial patterns and should be accepted or rejected together.

Rotation of the resulting eigenvectors has been advocated (e.g., Richman 1986; Cheng et al. 1995; O'Lenic and Livezey 1988) on the grounds that the rotated patterns are less likely to be influenced by sampling variations or the shape of the analysis domain and that they provide regionalized patterns with a simple structure, capable of a physically plausible interpretation. This technique has been used in a number of previous studies of the Northern Hemisphere circulation (e.g., Horel 1981; Hsu and Wallace 1985; Barnston and Livezey 1987) and by Kidson and Sinclair (1995) for the SH. In this case it may not be particularly appropriate, for the boundary of the analysis area is along a line where the variance is small and, where clear patterns of hemispheric extent exist, it is desirable to retain them. Varimax rotation of the variance-weighted EOFs (sometimes referred to as PCs) has been applied to most of the patterns obtained here and has been successful in some cases in separating overlapping modes.

3. Streamfunction climatology

The mean streamfunction patterns show a circumpolar vortex with a strong meridional gradient in midlatitudes. Latitudinal variations and departures from zonal symmetry are more easily seen in the zonal wind components derived from them. Figure 1 shows the expected pattern (e.g., Hurrell et al. 1998) of a strong polar jet in summer with speeds up to $35\ m\ s^{-1}$, complemented by a subtropical jet in winter that is strongest over the sector between 60°E and 120°W and reaches $44\ m\ s^{-1}$ north of New Zealand. The winter flow pattern also shows evidence of a double jet structure to the south of New Zealand. The standard deviation of the low-pass (IA) and bandpass (IS) filtered streamfunction is shown in Fig. 2, where it may be seen that these have similar amplitudes decreasing toward the equator and higher latitudes. The main departures from zonal symmetry

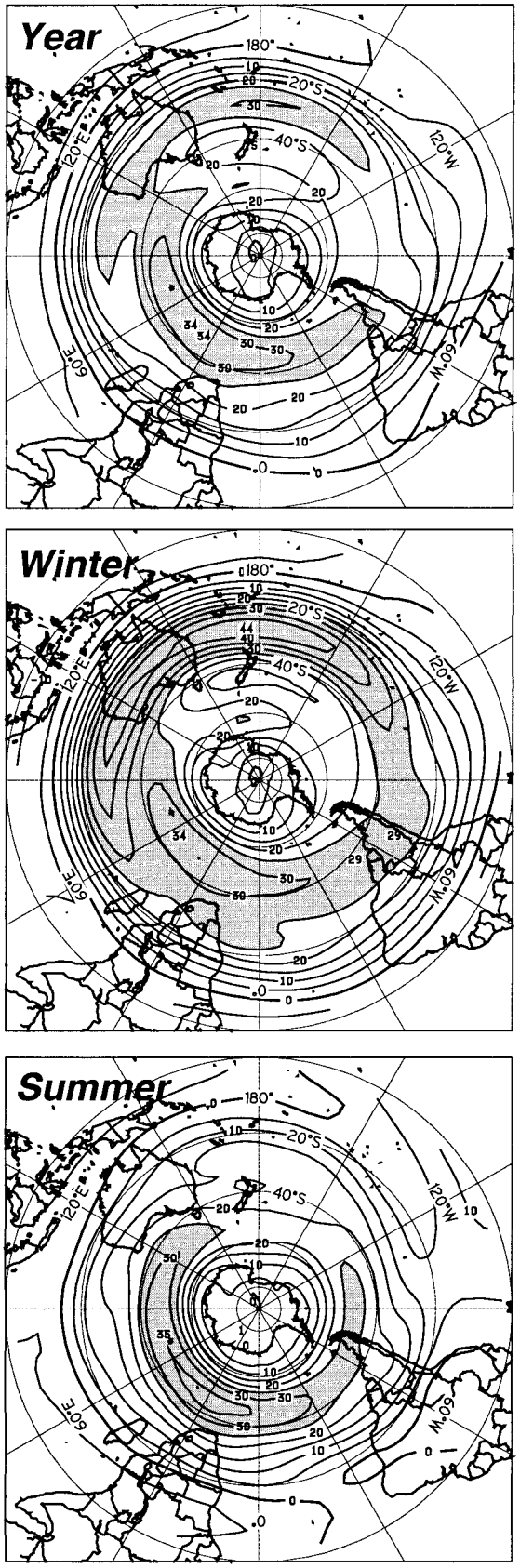

occur in each case in the Pacific sector, particularly for the low-pass filtered anomalies.

The interannual variance has been further partitioned into ID and interannual-monthly (IAM) components by taking 11-month running means of the low-pass filtered anomalies and by subtracting these from the individual monthly means. The 11-month averaging period gives an approximately equal division of the interannual variance between these two bands; sets an approximate 12-month period as the lower limit for ID variations; and, as an odd number, facilitates the differencing required for the IAM series. Monthly mean data were used for this part of the analysis as it is difficult to design filters to remove ultralow-frequency components from daily data.

The IAM component has maximum variance in the South Pacific as for the IA pattern, but at lower latitudes departures from zonal symmetry are small. The increase in variance at low and midlatitudes over the Pacific in the IA pattern is seen to result from the ID component, which is concentrated in this sector and makes a relatively small contribution to the variance over the remainder of the hemisphere. A comparison of the ID pattern with the Trenberth (1981) analysis of 500-hPa height field variance shows that for the 512–4096-day band, he also obtained a maximum between 20° and 30°S in the central Pacific, which is not present in the 64–512-day band. The 50-day low-pass variance shown by Kidson (1988b) also features a maximum southeast of New Zealand and overall is quite similar to the IAM pattern. Since it also is based on geopotential heights, it is not surprising that it fails to show the IA streamfunction peak in the tropical Pacific. The 10–50-day bandpass variance in Kidson (1991) also peaks near 50°S and has maximum amplitude southeast of New Zealand.

4. Intraseasonal variability

EOF analysis of the 10–50-day bandpass filtered data resulted in the six significant patterns shown in Fig. 3, which together account for 34.5% of the IS variance. These may be grouped into three pairs with similar explained variance. The leading modes, IS 1 and 2, represent orthogonal phases of a wavenumber-4 pattern aligned along the main SH storm track near 50°S (Trenberth 1991). While IS 3 and 4 appear dissimilar in Fig. 3, their contribution to the zonal wind variations, shown by their meridional gradient in Fig. 4, are seen to complement each other. Both gradient patterns have as their major contribution a wavenumber-4 intensification of

←

FIG. 1. Mean zonal wind component obtained from the 300-hPa streamfunction for the period Jan 1958–Jun 1997 averaged for all data and for the winter (Jun–Aug) and summer (Dec–Feb) seasons. Units: m s^{-1}.

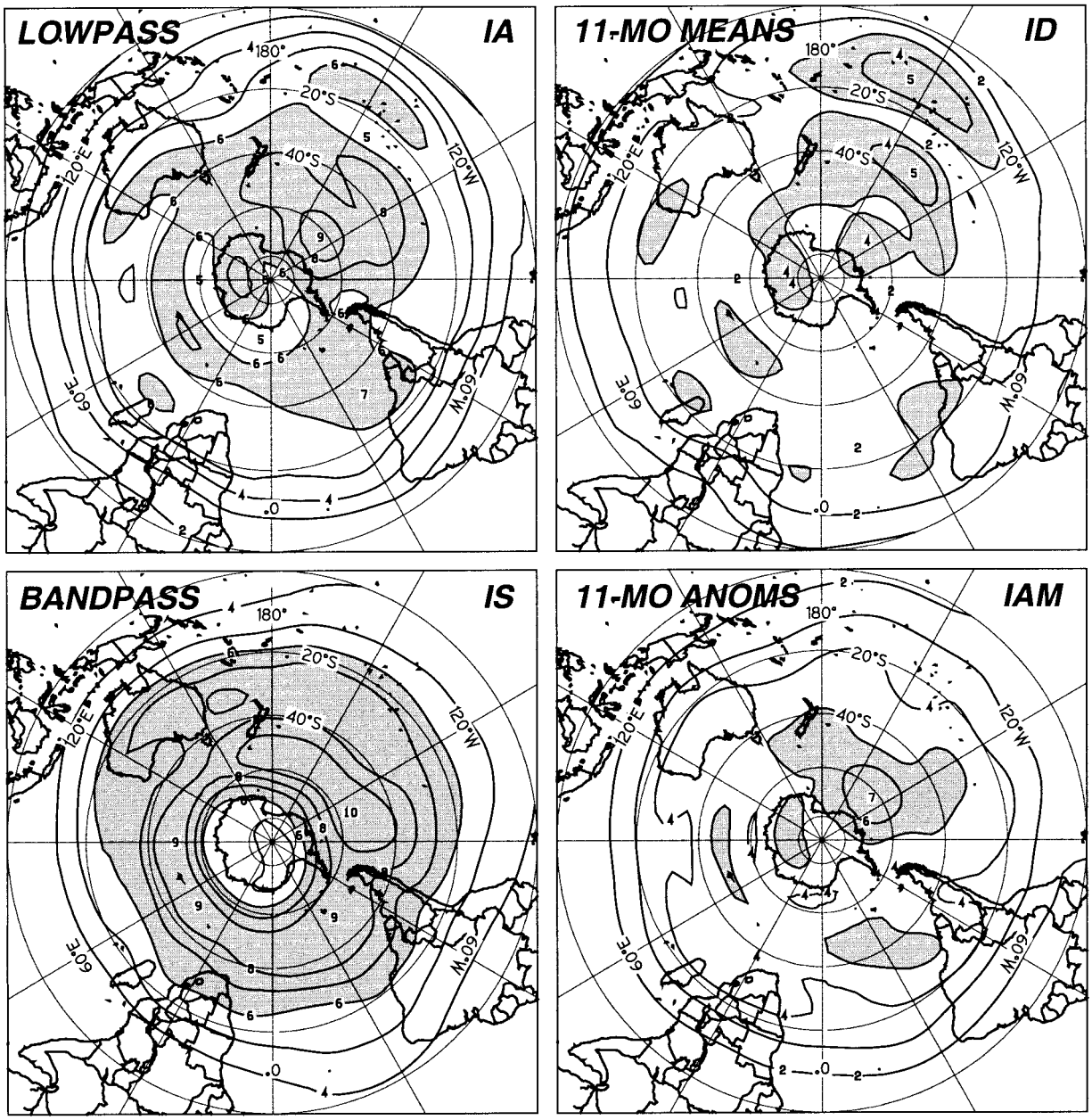

FIG. 2. Annual-mean standard deviation of the 300-hPa streamfunction after 10–50-day bandpass filtering (BANDPASS), 50-d low-pass filtering and removal of the annual cycle (LOWPASS), 11-month means of the low-pass filtered anomalies (11-MO MEANS), and deviations of the monthly means from the corresponding 11-month means (11-MO ANOMS). Units: 10^6 m^2 s^{-1}.

the zonal flow near 30°S, while the streamfunction patterns indicate a weak wavenumber-4 pattern at midlatitudes. Modes IS 5 and 6 are generally similar to 1 and 2 but show wavenumber 5 instead of 4 and lie, on average, farther north near 40°S.

Spectral analysis results in the expected broad peak near 15 days, the mean frequency passed by the bandpass filter. At this frequency IS 1 leads IS 2 by 90° in phase with coherency values in the range from 0.6 to 0.68. For a nominal 15-day period, this corresponds to eastward propagation of ~12° longitude per day, or ~10 m s^{-1} at 50°S. Mode IS 6 also leads IS 5 by 90° in

→

FIG. 3. The six leading EOFs of the annual intraseasonal (10–50 day) 300-hPa streamfunction variance.

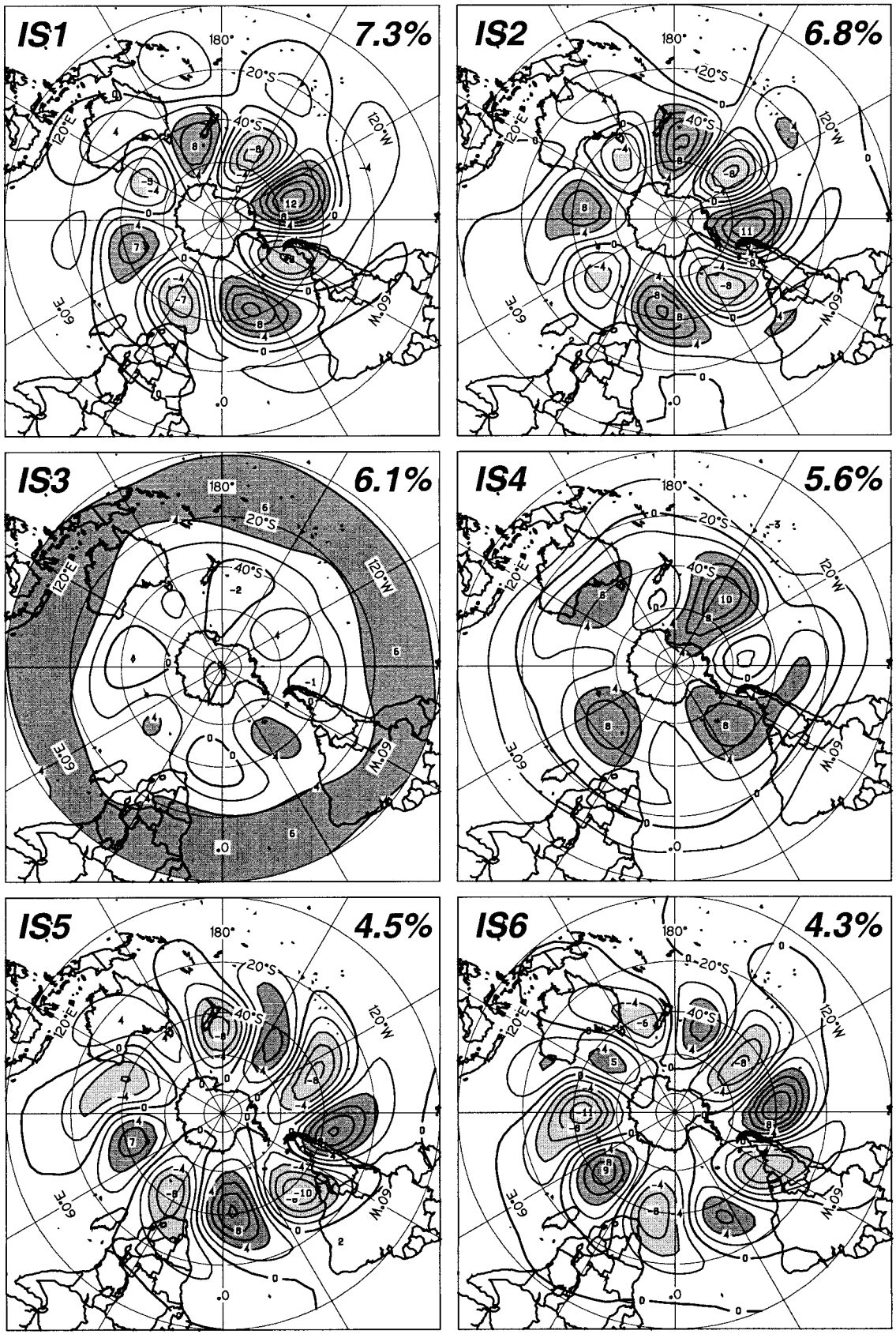
IS1
7.3%
IS2
6.8%
IS3
6.1%
IS4
5.6%
IS5
4.5%
IS6
4.3%
180°
20°S
40°S
120°E
120°W
60°E
60°W

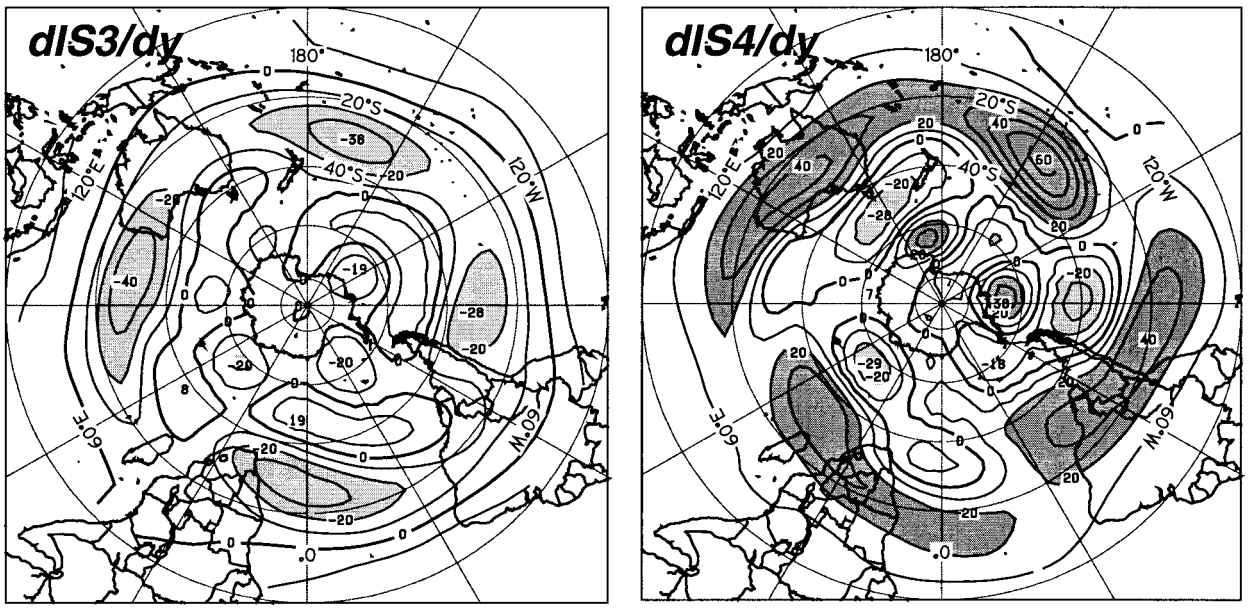

FIG. 4. The meridional gradient of IS3 and IS4 from Fig. 3.

phase with coherencies in the range 0.4–0.7 near the 15-day peak in the spectrum. This again can be interpreted as eastward propagation at a similar speed to the wavenumber-4 pattern represented by IS 1 and 2. Modes IS 3 and 4 are only weakly related in time with coherencies of order 0.25 and small phase differences in the main spectral band. We infer that there is no systematic progression between these two EOF patterns. Here IS 1 and 2 are very similar to the first two EOFs obtained by Kiladis and Mo (1998) from 500-hPa height fields from the same dataset from 1973 to 1996 except for a greater amplitude over the Atlantic and Indian Ocean sectors. There are no counterparts for their EOF 3 and 4 patterns among the unrotated EOFs.

To examine the seasonal variation of the patterns more closely, the EOFs were computed separately for winter (June–August) and summer (December–February), resulting in the leading EOFs shown in Figs. 5 and 6, respectively. In winter, only 2 EOFs appear to be significant and these show interleaved wavenumber-4

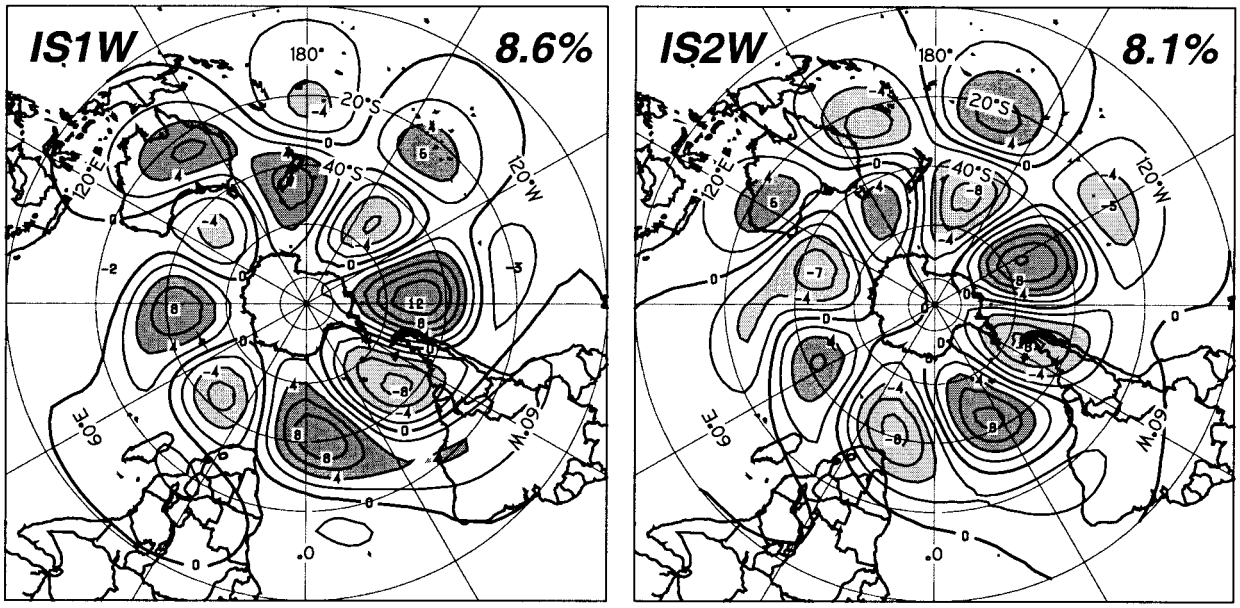

FIG. 5. The two leading EOFs of bandpass filtered 300-hPa streamfunction for winter (Jun–Aug).

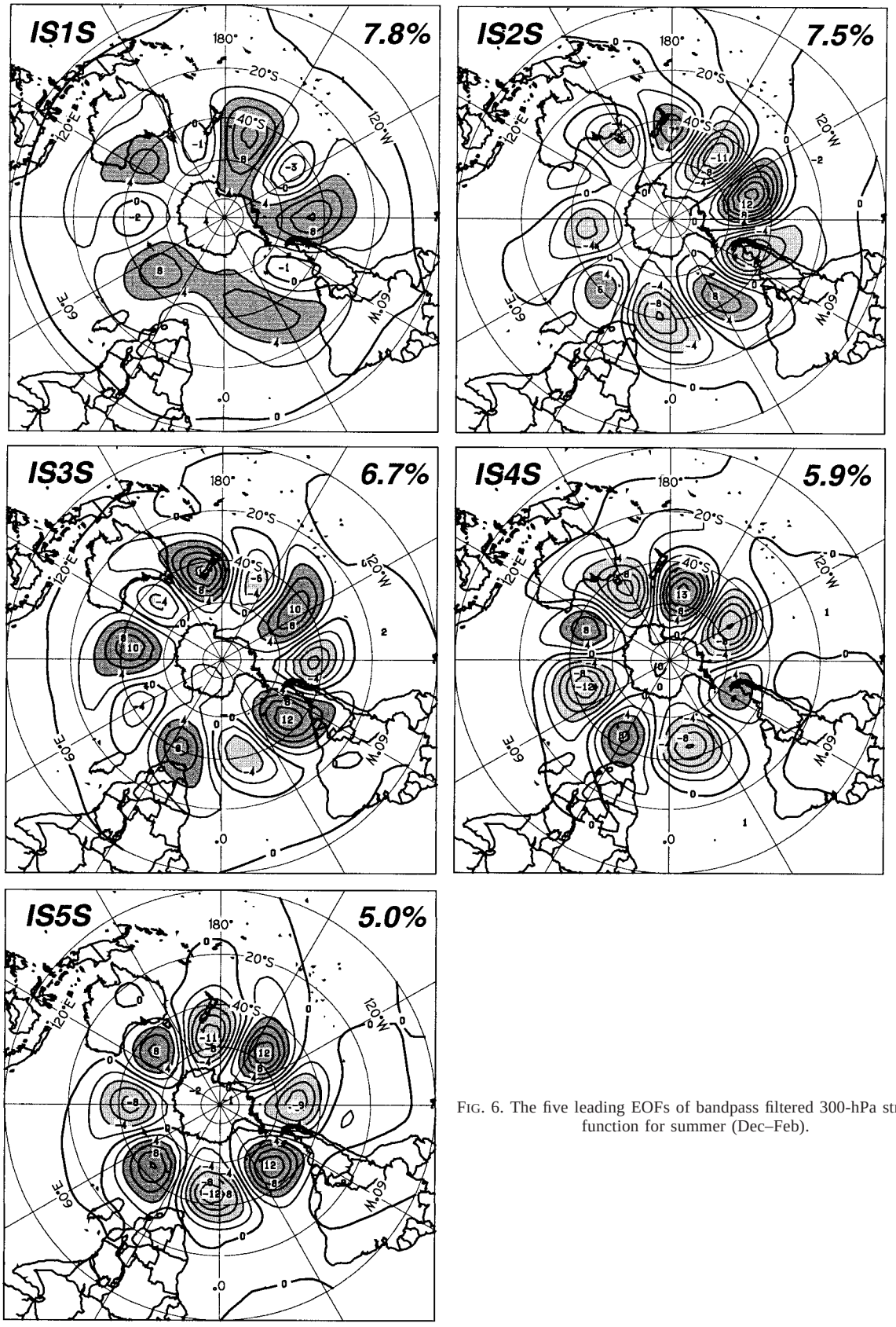

FIG. 6. The five leading EOFs of bandpass filtered 300-hPa streamfunction for summer (Dec–Feb).

patterns around the main storm track similar to the annual case. The main difference from IS1 and IS2 is that the winter patterns have centers of the opposite sign lying to the north over the Australian–Pacific sector. The variance explained by these two EOFs is 16.7%. In summer the wavenumber-4 pattern appears as IS4S and IS5S, but the wavenumber-5 pattern is now more prominent, appearing in IS1S, IS2S, and IS3S.

In contrast to the results of Kidson (1988a, 1991), there is no sign of the zonally symmetric high-latitude mode in the above analyses. This may be because the use of the streamfunction here gives more weight to variations in low latitudes; however, the Kiladis and Mo (1998) results from geopotential height also fail to show it. Another result that was unanticipated is the absence of any wavenumber-3 patterns. These appear in a number of earlier studies, though generally on longer timescales (e.g., Mo and White 1985; Mo and Ghil 1987). However, the evidence for wavenumber 3 in the Kidson (1991) and Kiladis and Mo (1998) results is not particularly strong, and Mo and van Loon (1984) and Mo and Higgins (1997) both comment that wavenumber 3 has strong secular variability and was much less prominent in the 1970s. The presence of wavenumber-5 patterns, and their dominance in the summer months, is consistent with the findings of Salby (1982) and Hamilton (1983) for the FGGE year 1979. It is also featured in the Kidson (1991) analysis for the summer months but is not present in the Kiladis and Mo (1998) analysis of the NCEP–NCAR 500-hPa height fields.

Kiladis and Mo (1998) present composites of streamfunction, wind, and height anomalies for large negative outgoing longwave radiation (OLR) departures in the 30–70 day band associated with the MJO. Their SH wintertime 500-hPa height anomalies show a similar pattern to the South Pacific wave train, and it appears that a substantial portion of the IS variability during winter is related to the MJO. The analysis of Mo and Higgins (1998) for the SH winter season suggests that the tropical and midlatitude intraseasonal modes may have different origins, but they do interact episodically. A strong tropical intraseasonal oscillation creates a favorable situation for the midlatitude pattern to intensify. In contrast, the analysis of the streamfunction field for the full year presented here shows that the principal IS wave trains for the 10–50-day band are confined to the polar vortex near 50°S. In winter there are links to tropical streamfunction anomalies of the opposite sign throughout the Australian–Pacific sector but little evidence for propagation from the Tropics.

5. Interannual variations

The variance explained by the leading EOFs of the 50-day low-pass filtered data is shown in Table 1. The first 5, for the entire 40-yr period, appear to be significant, and their spatial patterns are presented in Fig. 7. The leading EOF contributes 26.4% of the variance and represents zonally symmetric changes in the strength of the zonal wind near 25°–30°S. The gradients are small to the south of the streamfunction maximum near 30°–40°S.

TABLE 1. Fraction of variance explained by leading EOFs of 50-day low-pass filtered 300-hPa streamfunction for the indicated range of years, and for summer (DJF) and winter (JJA) for the entire period.

EOF	1958–97	1958–77	1978–97	1980–86	DJF	JJA
1	0.264	0.238	0.301	0.333	0.390	0.226
2	0.091	0.096	0.091	0.085	0.099	0.108
3	0.066	0.071	0.061	0.067	0.069	0.076
4	0.052	0.061	0.057	0.058	0.045	0.074
5	0.048	0.053	0.042	0.049	0.041	0.051
6	0.037	0.042	0.037	0.040	0.033	0.046
7	0.035	0.037	0.035	0.035	0.029	0.038
8	0.031	0.032	0.030	0.032	0.026	0.032
9	0.028	0.028	0.027	0.028	0.022	0.030
10	0.025	0.026	0.024	0.025	0.019	0.027

Modes IA 2 and 3 show a mixture of the high-latitude mode and zonally oriented patterns over the central Pacific that, as we will see in section 7b, are strongly related to ENSO. The main difference between these two EOFs is the phase of the HLM relative to the ENSO pattern. Modes IA 4 and 5 essentially capture the SPW, though both contain elements of variation in strength of the subtropical jet.

Rotation of these EOFs is able to provide a clear separation of the ENSO and HLM patterns but does not help the interpretation of the SPW pattern. It was carried out for the five significant EOFs weighted by their contribution to the variance, and also for the leading 7 and 11 patterns where the scree test suggested divisions might be made. The leading 5 rotated patterns, IA R1–5, shown in Fig. 8, were present in each set of rotated EOFs and are apparently not sensitive to over- or underrotation (O'Lenic and Livezey 1988). Here IAR1 is principally an indicator of the strength of the zonal wind along a band spiraling southward from 10°S over South America, to nearly 20°S over Australia, and 25°S over the central Pacific. The IAR2, which has a major contribution from the sum of IA2 and IA3, has isolated the classic HLM pattern; and IAR3, which has a substantial component from IA3 minus IA2, depicts the ENSO mode. While IAR5 retains a substantial contribution from IA5, the SPW is less clearly seen after rotation.

a. Stability of EOF patterns

The stability of the EOF patterns in Fig. 7 has been checked by partitioning the dataset into two halves, 1958–77 and 1978–97; and the data for 1980–86 only have also been analyzed for comparison with the Kidson (1988b) results from ECMWF data. The variance reductions from the leading EOFs are shown in Table 1. The scree test suggests that the first five should be selected in all cases except 1978–97 where EOF 5 may not be significant. It should be included, however, as it

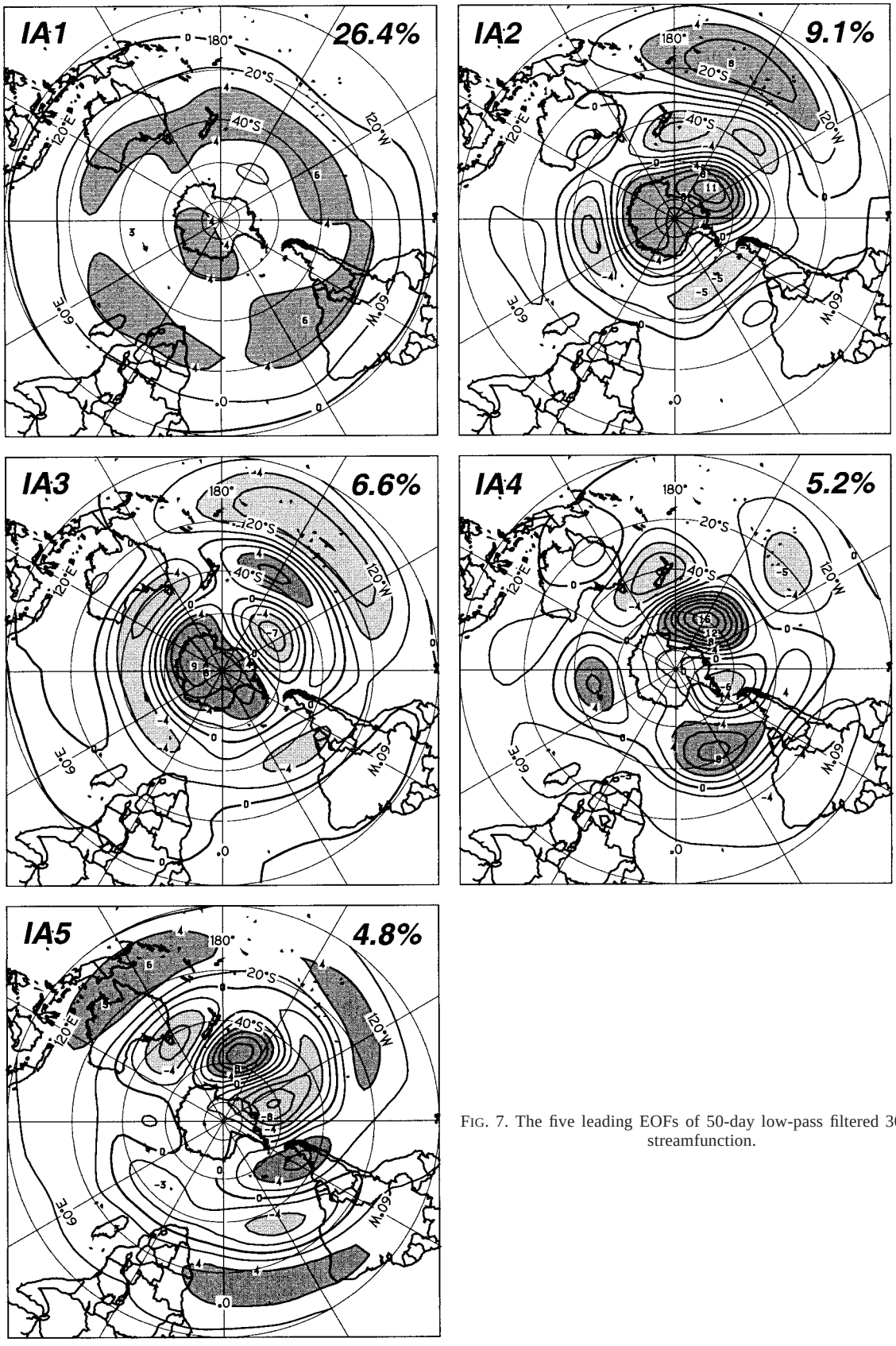

FIG. 7. The five leading EOFs of 50-day low-pass filtered 300-hPa streamfunction.

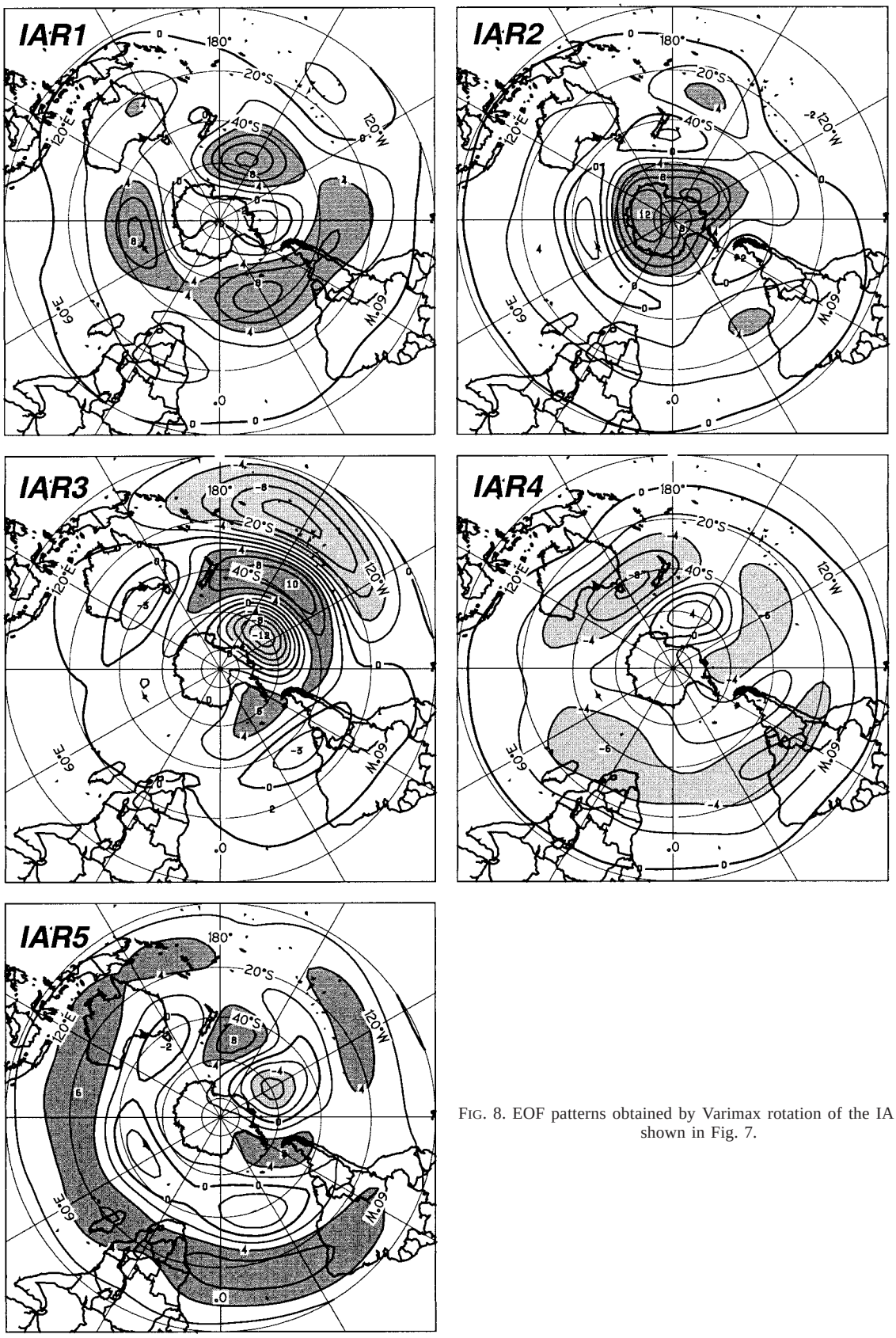

FIG. 8. EOF patterns obtained by Varimax rotation of the IA EOFs shown in Fig. 7.

again contributes one of the SPW patterns. The contribution of EOF 1, the tropical mode, is greatest for the 1980–86 period and raises the total variance explained by EOFs 1–5 to 59%, compared to 52% for the entire 40-yr record. The patterns in each case are generally similar to those in Fig. 7, with EOF 1 representing low-latitude zonal wind variations, EOFs 2 and 3 a mixture of the ENSO and HLM patterns, and EOFs 4 and 5 the SPW. The location of the interleaved SPW maxima varies somewhat between the analysis periods, but they lie along the same path.

b. Seasonal variations

The leading EOFs for winter (June–August) and summer (December–February) are shown in Figs. 9 and 10. The scree test applied to the variance reductions shown in Table 1 suggests that only the four leading EOFs are significant in winter and three in summer. However, the coherent three-wave patterns at higher latitudes in IA5W and IA6W, and IA4S and IA5S that represent the SPW in summer, are in line with previous analyses and should also be retained. The overall variance reduction is greater in summer, largely due to the 39% contributed by IA1S, which has a very similar pattern to the annual EOF, IA1. The remaining summer patterns, IA2S–IA5S, differ in some details from the annual patterns in Fig. 7 but essentially show the same features—mixtures of the ENSO and HLM patterns, and the SPW.

The leading EOF for winter, IA1W, is again similar to the annual pattern IA1 and accounts for a similar fraction of the variance. The HLM and ENSO patterns in IA2W and IA3W are better separated than for the year as a whole and for the summer, with the HLM-dominated pattern IA2W accounting for a greater fraction of the variance. The remaining three patterns, IA4W–IA6W, show evidence of wavenumber-3 patterns at higher latitudes and a tendency for reversal of the anomaly centers near 20° and 40°S. The SPW stands out less clearly than in the annual and summer patterns. Rotation of these patterns (not shown) again separates the ENSO and HLM patterns but does not otherwise help the interpretation.

c. Comparison with previous results

The recent analysis of Kiladis and Mo (1998), based on 500-hPa heights from the same dataset for 1973–95, reproduces some of the same EOFs but fails to reveal the tropical linkages shown by the ENSO pattern, or the low-latitude zonal wind variations of IA1. Their first EOF with 25% of the variance provides a clear representation of the HLM, corresponding to IAR2. Their second EOF depicts the higher-latitude portion of the ENSO mode in IAR3 but lacks the tropical lobe due to the smaller variance of the geopotential height field at low latitudes. Their third EOF is a good match to IA4 (without the tropical components), but their fourth is unlike any of those presented here.

Three EOFs were obtained from normalized 500-hPa height departures from the Australian dataset with zonal filtering by Mo and Ghil (1987). The first is readily identifiable as the HLM, and the remaining two show patterns with a substantial wavenumber-3 component at middle and higher latitudes. The pattern of three centers in EOF 3 near South America was referred to as the Pacific–South American pattern, but neither their second nor third EOF contains a good representation of the SPW as obtained elsewhere. Subsequent results from Farrara et al. (1989) used 500-hPa heights from the National Meteorological Center (now the National Centers for Environmental Prediction) dataset for SH winters between 1979 and 1985 without any time filtering. Two of their EOFs contain representations of the HLM and one phase of the SPW (cf. IA5), but the others are more reminiscent of IS patterns.

Kidson's (1988b) analysis provided three significant EOFs from the height field covariance, representing the HLM and SPW patterns derived here. The first EOF from standardized 500-hPa height anomalies, contributing 23.4% of the variance, is similar to IA1 and has a zonally symmetric pattern with strong gradients near 20°S. His second and third EOFs provide a clear representation of the SPW.

A more direct comparison is possible with the global streamfunction EOFs of Lau et al. (1994). Their first EOF is zonally symmetric and accounts for 22.7% of the total variance. It shows strong meridional gradients in the subtropics of both hemispheres and evidently corresponds to the ''tropical'' mode, IA1. Their rotated EOFs 7 and 8, referred to as PSA-1 and PSA-2, are largely confined to the SH and contain a good representation of the SPW as shown in Figs. 7 and 8. Their interannual mode (REOF1) shows a double cell structure in the Tropics whose Southern Hemisphere portion matches the subtropical center in the ENSO mode but fails to show the linkages to higher latitudes revealed in this study. Their global analysis has also failed to reveal the Southern Hemisphere HLM.

6. Intradecadal variations

In order to separate intradecadal variations with periods of 12 months and more, an 11-month running mean was applied to the monthly means of the low-pass-filtered streamfunction anomalies with the annual cycle removed. The 11-month running means were also subtracted from the individual monthly means to provide an alternative IA analysis for variability in the range 2–11 months. As seen in Fig. 2, the variance in each of these low-frequency bands is comparable, but on the ID timescale most is concentrated in the Pacific where it extends to lower latitudes than for the shorter timescales.

EOF analysis of the 11-month running mean series

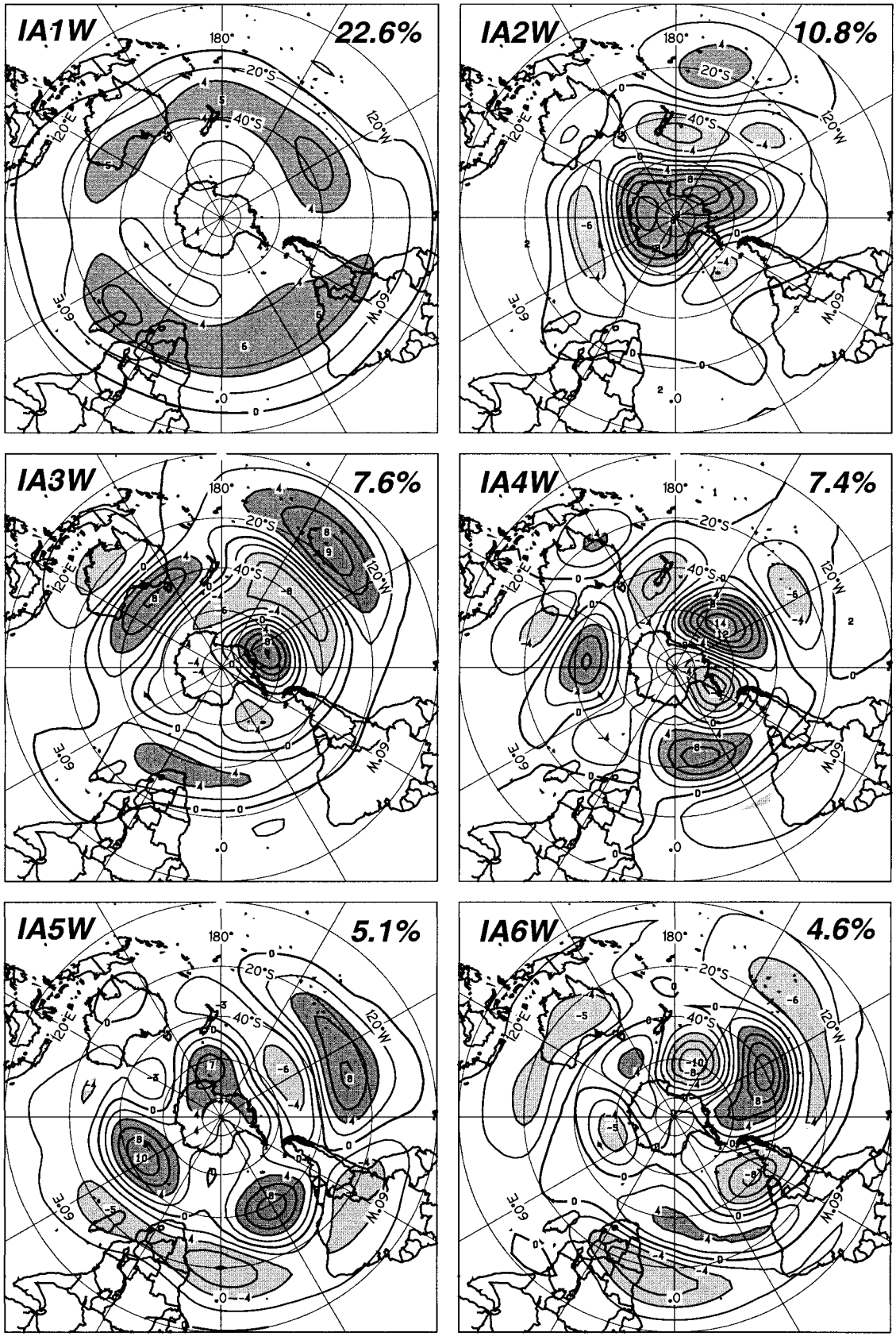
IA1W
22.6%
IA2W
10.8%
IA3W
7.6%
IA4W
7.4%
IA5W
5.1%
IA6W
4.6%
180°
20°S
40°S
120°W
120°E
60°E
60°W

produced five significant patterns, which are shown in Fig. 11, contributing 74% of the variance. The ID1 is similar to IA1, while ID2 and ID3 show mixtures of the ENSO and HLM patterns, and ID4 a wave train extending from the tropical Pacific through high latitudes to the tropical Atlantic. Rotation of these five EOFs (Fig. 12) provides a good match with the ENSO and HLM patterns, IAR2 and IAR3, and with the lower-latitude patterns of IDR2 and IAR5. The wavenumber 3–4 pattern in IAR1 is less prominent in IDR1, and its maximum amplitude is displaced slightly to the north. The IDR5 has no counterpart in the IA band, but it appears to complement the ENSO pattern with its centers of action lying between those of IDR4.

For the IA component of the low-frequency variance, the first four EOFs, which contribute 45.6% of the variance in this band, are presented in Fig. 13. These show the variability in tropical winds featured in IA1, the HLM pattern isolated by IAR2, and two SPW patterns modulated by a zonal wavenumber-3 pattern near 50°S. The ENSO pattern is absent on this timescale.

7. Low-frequency variability and trends in the 1957–97 period

Time series of individual EOFs show both low-frequency variations and secular trends on the ID timescale over the 40-yr record. Those for ID EOFs 1–3 (ID1–ID3), obtained by mapping these patterns onto monthly means of the 50-day low-pass filtered streamfunction anomalies, are shown in Fig. 14. The high-frequency variation has largely been removed by the application of a 12-month running mean to each series.

The time series of the SOI which has been computed from the normalized pressure difference between Darwin and Tahiti, is also shown, and the strong negative correlation between it and the series for ID1 is immediately apparent. The main feature of the series for ID2 is a secular change, with the low values before 1970 generally outside the range subsequently observed. Similar upward trends are found in the time series for IA2 and IA5, and a matching downward trend in IA4 (not shown). The series for ID3, which represents the HLM, has low values and longer period fluctuations in the decade centered on 1970 and a persistent positive departure centered on 1995. Otherwise its year to year variations appear to be small. The variations in ID1 and ID2 are examined in more detail below.

a. Circulation differences prior to 1970

The year 1970 has been taken as an arbitrary break point to evaluate the changes in the circulation implied by the ID2 time series. The differences in mean streamfunction from 1958–69 to 1970–97, and the zonal wind component derived from it, are shown in Fig. 15. From the close resemblance of this difference pattern to ID2 in Fig. 11, it is apparent that this EOF has captured much of the circulation difference between these two periods. These show a strong wavenumber-2 pattern in the zonal wind change poleward of 20°S, and an increase is observed in the equatorial westerly component over the western and central Pacific. While the anomaly pattern is suggestive of southward displacements of the subtropical jet over the central Pacific and the polar jet over the Indian Ocean after 1970, the mean fields essentially show a weakening of the jets in the latter period.

Swanson and Trenberth (1981) have previously described changes occurring in the SH between 1957–66 and 1972–78 based on a comparison of Australian Weather Bureau analyses with those from the South African Weather Bureau used in the first American Meteorological Society Southern Hemisphere monograph (Newton 1972). Over the latter period the 500- and 200-hPa heights show increases at the pole and decreases in the Tropics. The pattern over the Indian Ocean is somewhat confused, but over the Pacific there appears to be a consistent increase in geopotential height north of 25°S and decreases to the south extending as far as 55°–60°S. The net effect is to increase the zonal wind near 20°–30°S in the central Pacific during the 1970s. The opposite trend is observed here and is more likely to be correct because it is based on a single homogeneous dataset. It is similar to, but does not appear to be linked with, the relatively abrupt change in the North Pacific observed a few years later by Trenberth and Hurrell (1994). Other significant changes occurred in the SH circulation in the late 1970s (e.g., van Loon et al. 1993; Chen and Yen 1997), but there is no evidence of them in the time series obtained here.

Some support for the changes in ID2 observed here is provided by a 35-yr control run of the Hadley Centre's unified model, forced by observed sea surface temperatures and sea ice distribution for 1961–95 (Kidson et al. 1998, unpublished manuscript). The second intradecadal EOF obtained from the model fields had a similar spatial pattern, and its time series also showed a discontinuity occurring near 1970.

b. ENSO linkages

The correlation between monthly values of the SOI and ID1 is −0.74, and, not surprisingly, we find similarities between the spatial patterns of ID1 and the correlation between streamfunction and the SOI shown in Fig. 16. The SOI and ID1 series are not completely independent, as the SOI is based on the MSL pressure

←

FIG. 9. The six leading EOFs of low-pass filtered 300-hPa streamfunction for winter (Jun–Aug).

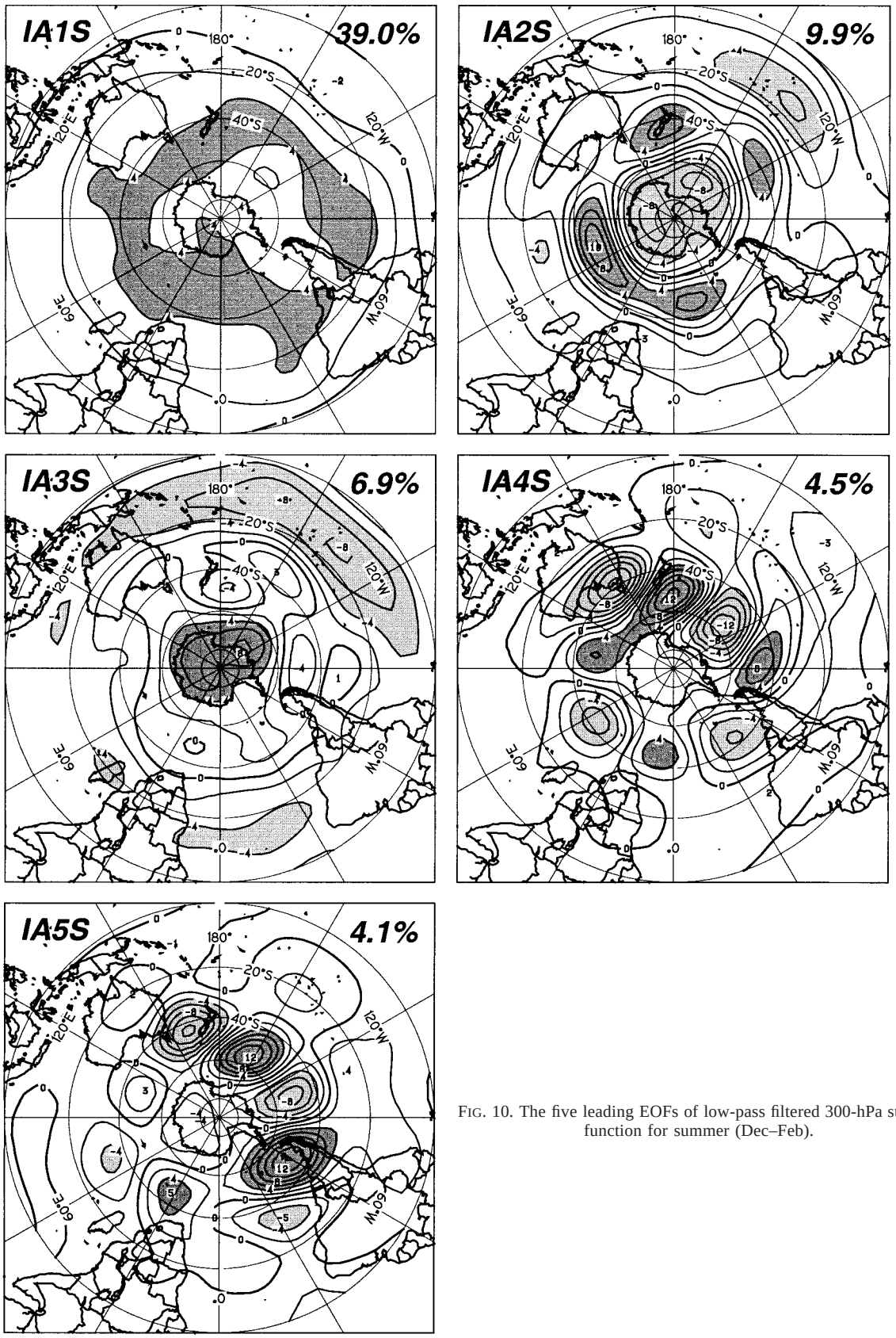

FIG. 10. The five leading EOFs of low-pass filtered 300-hPa stream-function for summer (Dec–Feb).

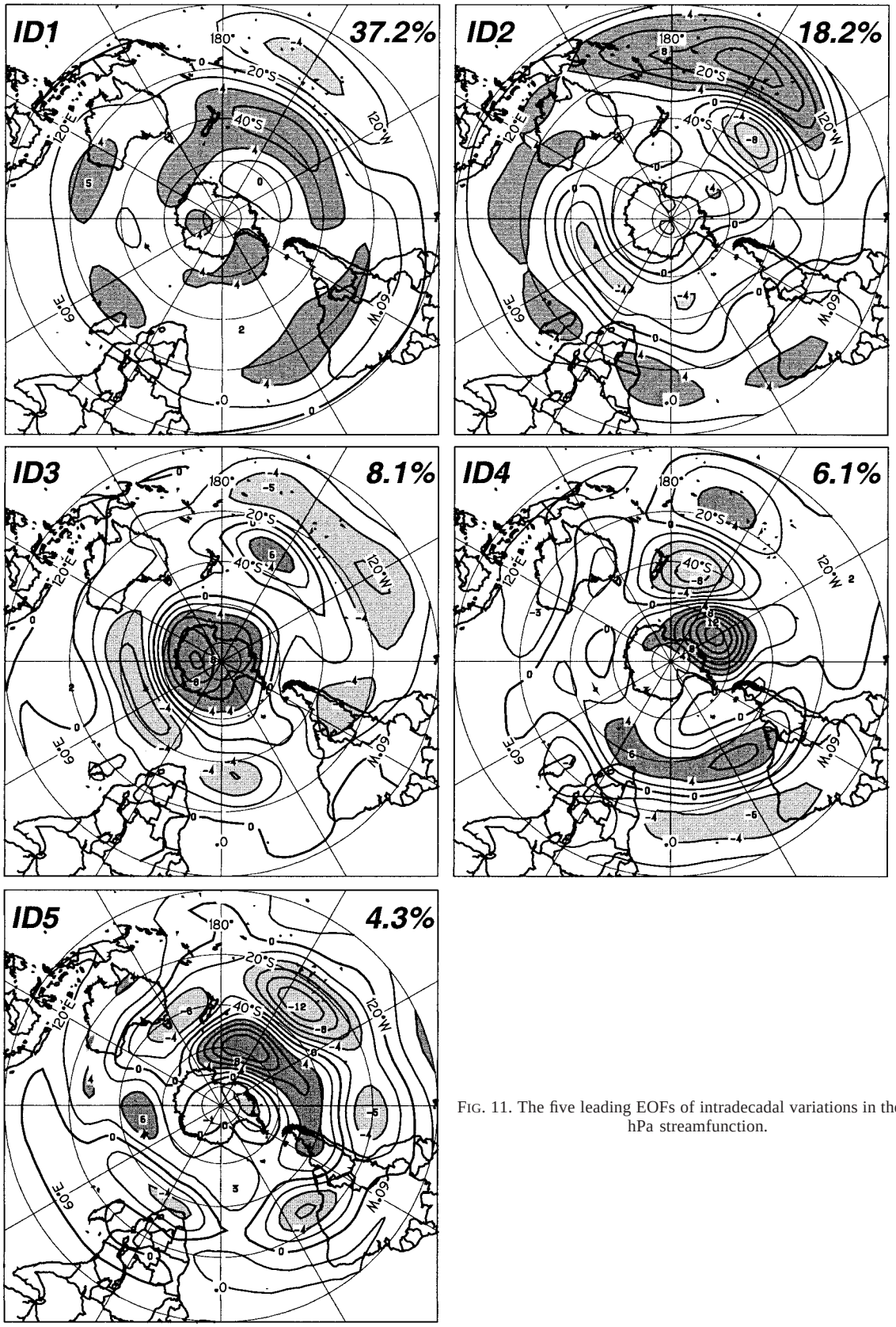

FIG. 11. The five leading EOFs of intradecadal variations in the 300-hPa streamfunction.

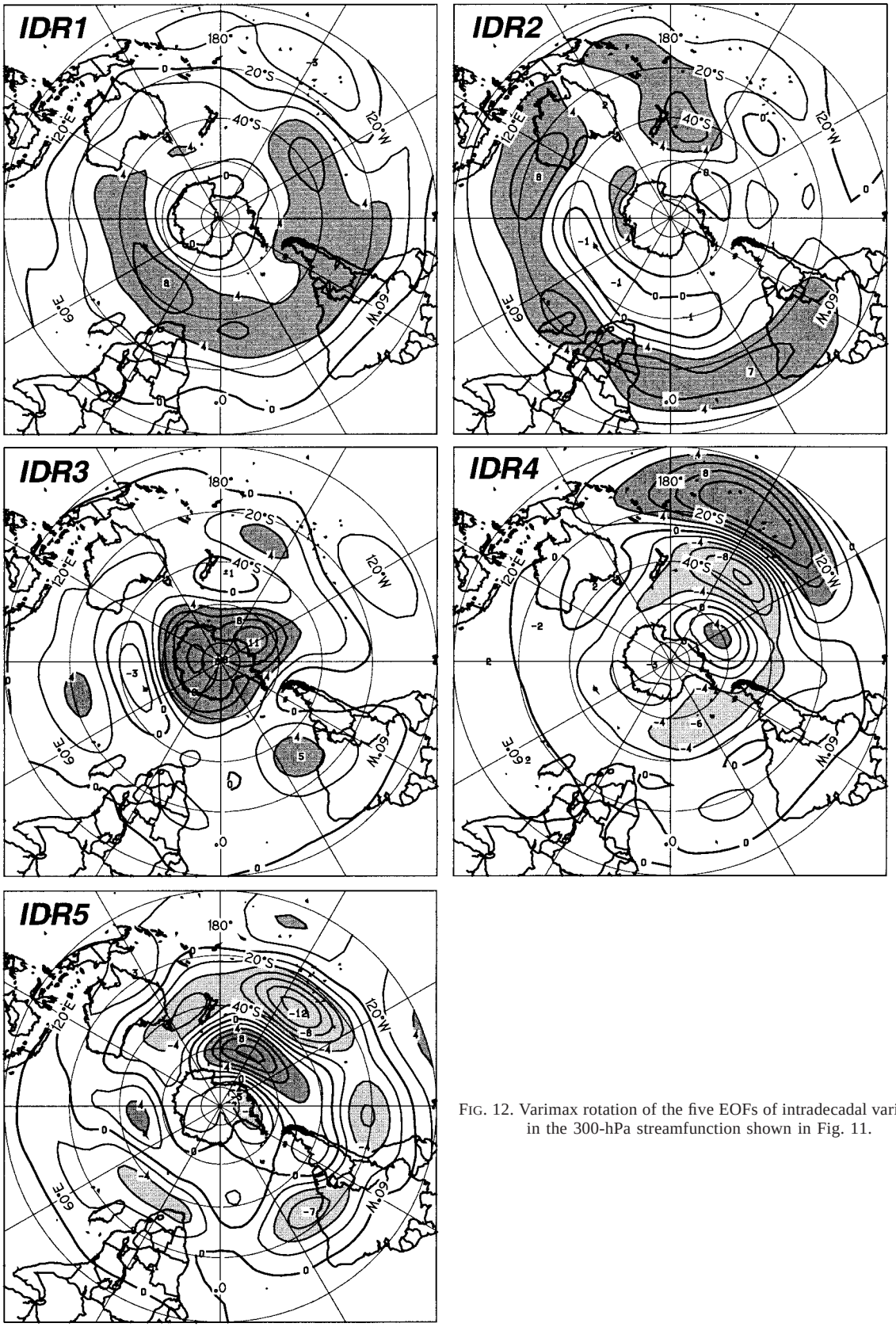

FIG. 12. Varimax rotation of the five EOFs of intradecadal variations in the 300-hPa streamfunction shown in Fig. 11.

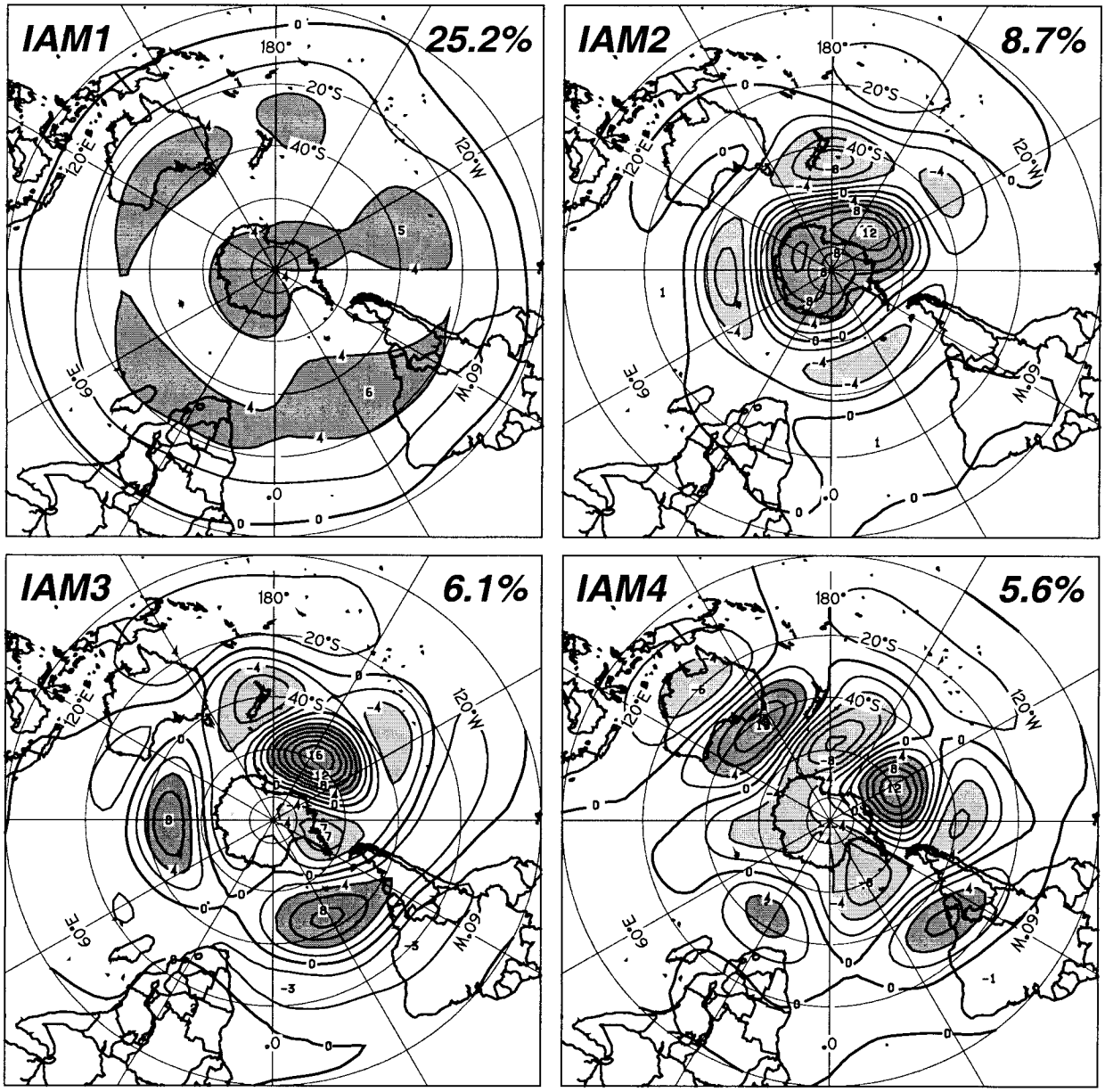

FIG. 13. The four leading EOFs of the 2–11-month variations in the 300-hPa streamfunction.

difference between Tahiti (17.6°S, 149.6°W) and Darwin (12.4°S, 130.9°E), which lie under opposing streamfunction anomalies. There are, however, no local maxima in the correlation field centered on these two station locations, and we may assume that the strength of the relationship does not primarily result from vertical coupling.

Moderate to strong correlations between monthly values of the SOI and the 50-day low-pass filtered streamfunction anomalies are found in the Tropics and over the Pacific sector at midlatitudes. Their magnitudes exceed 0.6 in the centers near 10° and 35°S. The difference between streamfunction composites for SOI ≥ 1 and SOI ≤ -1 shows essentially the same pattern with the variations outside the Pacific sector given less weight. The zonal wind fields for the low and high index composites also show that the largest changes take place in the Pacific sector and that the departures for the positive index composites are approximately twice those for the negative composites. This should not be taken as evidence of a nonlinear response. When composites are taken for classes more than one standard deviation from the overall mean of the SOI during the 1958–97 period (-0.22), the zonal wind anomalies are only a little stronger for positive departures of the index.

A similar strong relationship between the SOI and

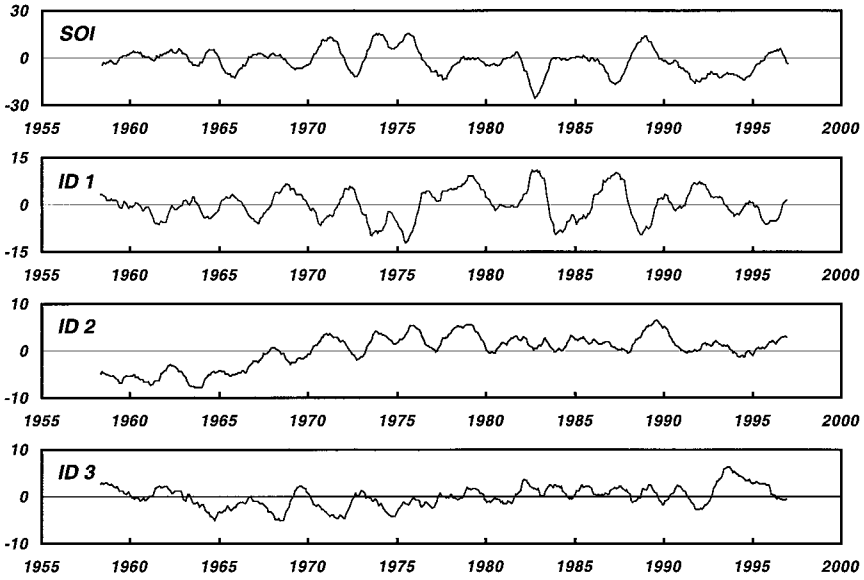

FIG. 14. Time series of the 12-month running mean of the Southern Oscillation index and of EOFs ID 1–3 mapped onto monthly mean low-pass filtered streamfunction.

monthly means of the IA R3 series is shown by the correlations in Table 2, indicating that rotation of the EOFs has effectively isolated this mode from its contributions to IA2 and IA3. EOF1 retains a moderately strong negative correlation in both its rotated and unrotated forms because the variations in the tropical zonal wind it portrays map onto the SOI pattern in ID 2. In their unrotated form the representations of the SPW in IA4 and IA5 are uncorrelated with the SOI.

The ENSO response pattern also appears in the earlier analysis of Kiladis and Mo (1998) and as the leading interannual mode in the global streamfunction EOFs of Lau et al. (1994). Each shows a symmetric pattern with complementary changes north of the equator and the presence of weaker patterns in the opposite phase over the Atlantic and Indian Ocean sectors. As with a number of Northern Hemisphere low-frequency patterns (Wallace and Gutzler 1981), the two main centers of the ENSO pattern straddle a jet exit region—in this case, the subtropical jet (Fig. 1). When sea temperatures rise

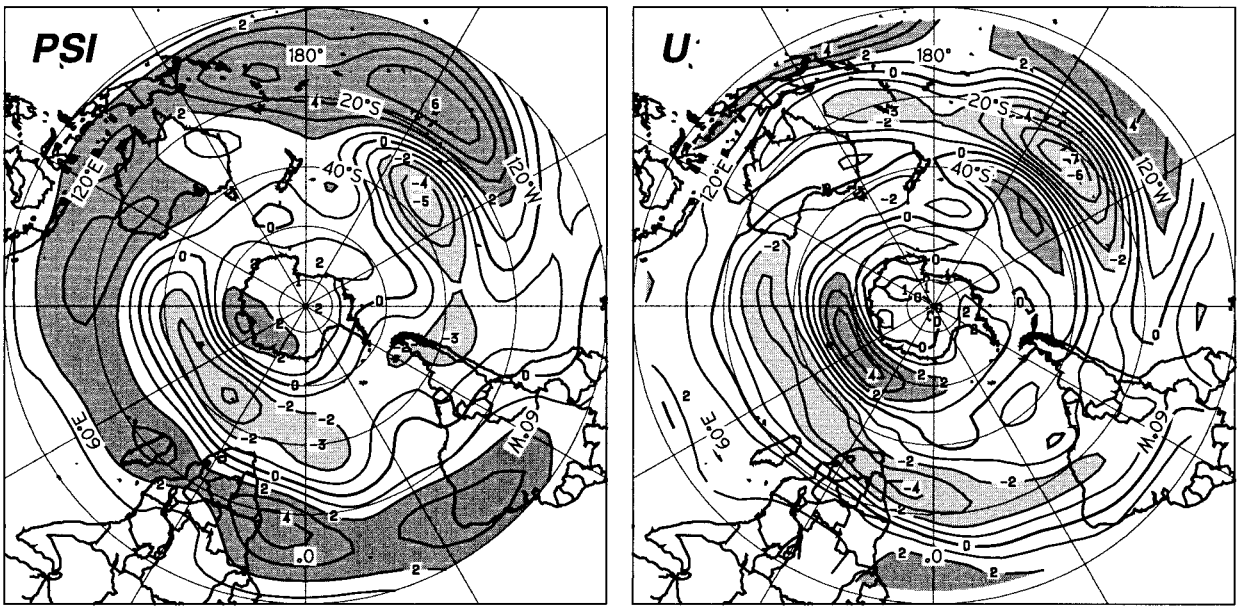

FIG. 15. The difference in mean streamfunction anomalies from 1958–69 to 1970–97 and the zonal wind difference derived from them.

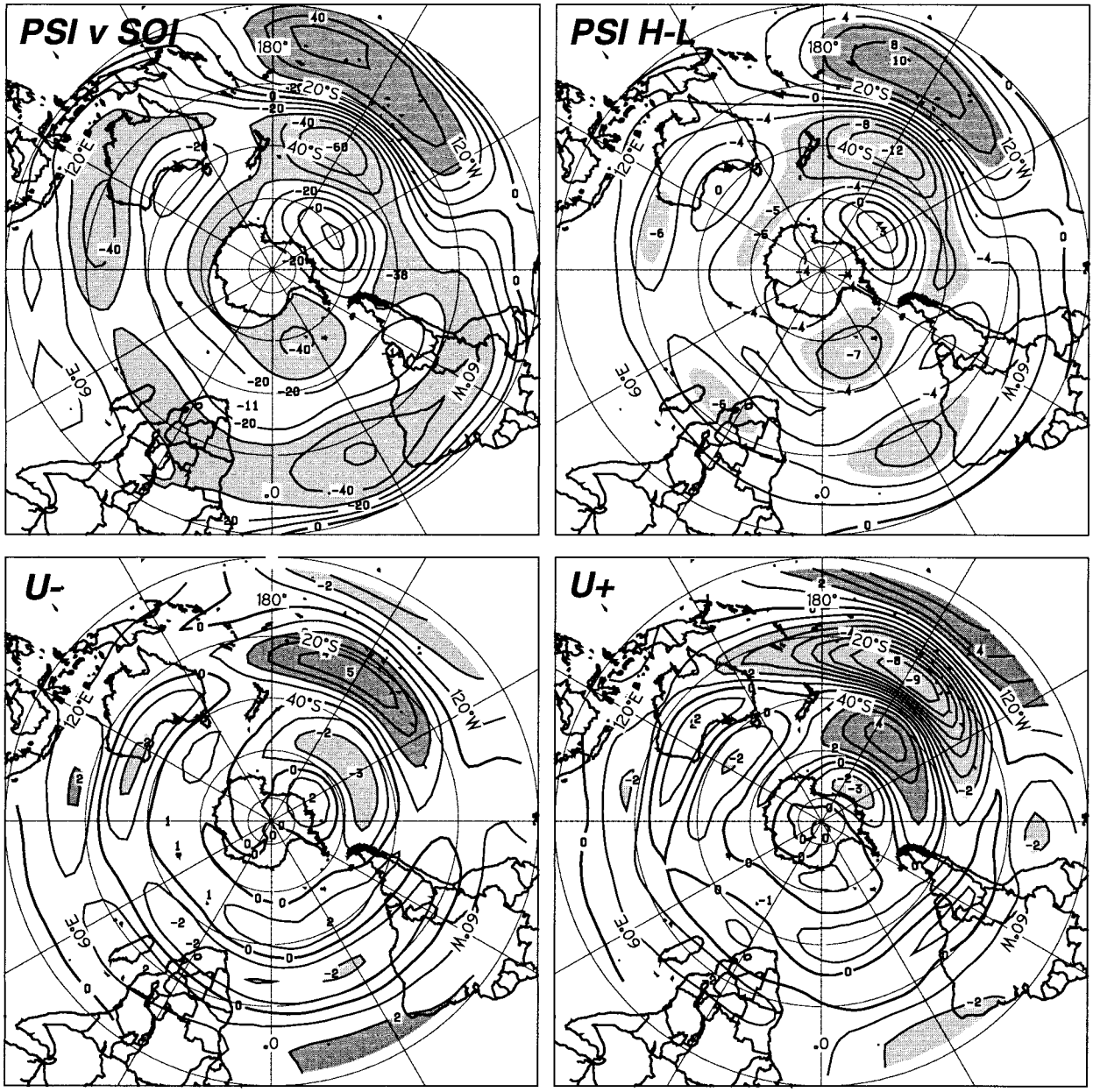

FIG. 16. The correlation between monthly mean SOI and 50-day low-pass streamfunction anomalies, difference between streamfunction composites for high ($>1\ \sigma$) and low ($<-1\ \sigma$) SOI, and zonal wind departures for low (U−) and high (U+) SOI values.

in the central Pacific, in association with a negative SOI, and convection spreads farther to the east along the equator (e.g., Kiladis and Mo 1998), we infer that the Hadley circulation is more intense in this sector. This would provide increased momentum transport to strengthen and extend the subtropical jet eastward, and it would provide a vorticity source for the ENSO wave train (cf. Rasmusson and Mo 1993). The orientation of this wave train slightly east of south is similar to the direction of propagation of Rossby waves with wavenumbers 1–3 in the northern winter obtained by Hoskins and Karoly (1981).

8. Discussion and conclusions

The results presented here update previous knowledge of low-frequency variability in the SH through extended coverage of a 40-yr period from the NCEP–NCAR reanalyses and through the use of the 300-hPa streamfunction to show more clearly the interactions with low latitudes.

While the distribution of the variance in the intraseasonal and interannual frequency bands shows similar patterns, with a high degree of zonal symmetry, the intradecadal component is concentrated in the Pacific, where it extends to lower latitudes.

TABLE 2. Correlations of the monthly mean SOI with the monthly mean values of the interannual EOFs IA 1–5 and IAR1–5 projected onto monthly mean streamfunction anomalies for the period 1958–97.

	1	2	3	4	5
IA	−0.46	0.26	−0.38	−0.05	−0.11
IAR	−0.46	−0.38	−0.59	0.40	−0.42

On the intraseasonal timescale (10–50 days), the principal modes revealed by EOF analysis show wavenumber-4 and -5 patterns largely confined to the main SH storm track near 50°S. Variations in the strength of the zonal wind near 30°S also appear on this timescale, but there is little evidence of a link between the tropical and midlatitude circulation. The wavenumber-5 patterns become more prominent during summer and, in contrast to earlier work, there is no sign of the high-latitude mode.

On the interannual timescale, including all variations with periods over 50 days, the leading modes show variations in the strength of the zonal wind in the Tropics, the high-latitude mode, an ENSO mode, and the South Pacific wave train. Similar patterns are observed during summer, but in winter, hemispheric wavenumber-3 patterns become more prominent at the expense of the SPW.

Separation of the low-frequency variations into components with periods above and below 11 months shows that the ENSO mode appears only on the intradecadal timescale, while the tropical mode and the SPW are confined to the interannual timescale. The ID timescale also reveals a ''trend'' pattern as its second EOF. This largely expresses changes taking place prior to 1970 and makes only a small contribution to the variance after that date.

The principal patterns associated with each frequency band are summarized in Fig. 17. The ''internal'' modes refer to the IS patterns that appear to be generated in, and propagate around, the principal midlatitude storm track (Trenberth 1991). The HLM is present on both IA and ID timescales but failed to feature in the IS analysis, contrary to the earlier analyses of Kidson (1988a, 1991). The SPW (or PSA) mode has previously been linked to variations in tropical convection associated with the 30–70 day Madden–Julian oscillation (e.g., Karoly 1989; Berbery and Nogues-Paegle 1993; Mo and Higgins 1998) and should therefore extend into the low-frequency end of the IS band. The ENSO mode is prominent only on the ID timescale where it matches the SH response obtained by Kiladis and Mo (1998) and the SH portion of the global pattern obtained by Lau et al. (1994). It is concentrated in the Pacific and is distinct from the zonally symmetric mode (e.g., Lau et al. 1994; Mo and Higgins 1998), which is important on the IS and IA timescales. The fraction of variance contributed by the leading modes increases with the range of periods, from 35% on the intraseasonal timescale to 74% for periods greater than 11 months. As seen in Fig. 2,

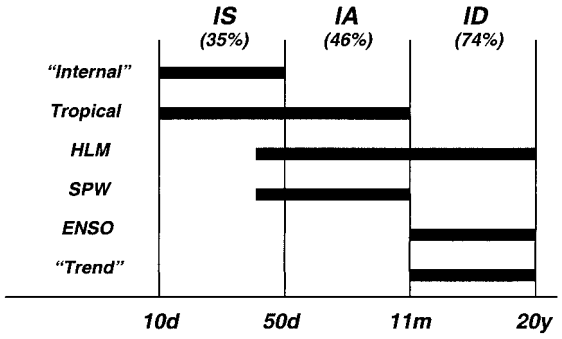

FIG. 17. Timescales associated with modes identified by EOF analysis. The IS, IA and ID bands have been delineated in this study by periods of 10 day, 50 day, 11 month and 20 yr (the upper limit represented in the 40-yr study period). The percentages indicate the proportion of variance in each band accounted for by the leading EOFs.

the overall variance in each of these three bands had a similar magnitude. This has implications for potential predictability in each frequency band. Another point to be made from this figure is the different mix of patterns within each band, indicating a need for prefiltering in further studies of this type.

The results presented here largely complement earlier studies of low-frequency variability based on analysis of SH geopotential height fields and global streamfunction analyses. The ''tropical'' and ''ENSO'' modes have low-latitude components that were generally not identified in previous SH analyses, but they agree well with the SH portions of global patterns obtained from streamfunction analysis. Evidently restricting the analysis domain has not caused any distortion in the global patterns and it has allowed a greater concentration on SH patterns. Time series of the EOF coefficients have shown that the 40-yr data series is homogeneous, but there may have been a significant change in the circulation before 1970. This is distinct from the widespread changes found in the late 1970s (e.g., van Loon et al 1993) and is similar to the changes observed in the North Pacific a few years later by Trenberth and Hurrell (1994). While there is some concern that the shift in the strength of the jets observed here may have resulted from inhomogeneities in the data, it is supported by the analysis of the unified model control run reported by Kidson et al. (1998, unpublished manuscript). This run is entirely independent of any atmospheric data, and it is presumed that the similar variation that it shows must result from the sea temperature forcing.

As with Lau et al.'s (1994) global streamfunction analysis, we have concentrated on the large scale, and there may be some regional patterns of interest that contributed insufficient variance to be identified by the EOF analysis. On the IA timescale, for example, we might perhaps have anticipated SPW-like wave trains originating from other heat sources in the Tropics (e.g., Yanai and Tomita 1998). On the ID timescale there has been no sign of the wavenumber-2 pattern with a 4-yr

period found by White and Peterson (1996) in sea temperatures and surface pressure analyses since 1982.

The results obtained from this new dataset are, of course, only another step in the continuing process of establishing the causes and predictability of low-frequency variability in both hemispheres. Observational and theoretical studies have done much to examine the role of tropical forcing (see reviews by Trenberth et al. 1998; Kiladis and Mo 1998), but much remains to be done to clarify the reasons for year to year variations both from this source and from boundary forcing at higher latitudes.

Acknowledgments. Thanks are due to Jim Renwick for his help in processing the NCEP–NCAR dataset and to the New Zealand Foundation for Research, Science and Technology for its support under Contract CO1628. Thanks are also due to Jim and to George Kiladis for comments on an earlier draft of the manuscript and to Glenn White and an anonymous reviewer for their helpful suggestions.

REFERENCES

Ambrizzi, T., B. J. Hoskins, and H.-H. Hsu, 1995: Rossby wave propagation and teleconnection patterns in the austral winter. *J. Atmos. Sci.,* **52,** 3661–3672.

Barnston, A. G., and R. E. Livezey, 1987: Classification, seasonality and persistence of low-frequency atmospheric circulation patterns. *Mon. Wea. Rev.,* **115,** 1083–1126.

Berbery, E. H., and J. Nogues-Paegle, 1993: Intraseasonal fluctuations between the Tropics and extratropics in the Southern Hemisphere. *J. Atmos. Sci.,* **50,** 1950–1965.

——, ——, and J. D. Horel, 1992: Wavelike Southern Hemisphere extratropical teleconnections.. *J. Atmos. Sci.,* **49,** 155–177.

Chen, T.-C., and M.-C. Yen, 1997: Interdecadal variation of the Southern Hemisphere circulation. *J. Climate,* **10,** 805–812.

Cheng, X., G. Nitsche, and J. M. Wallace, 1995: Robustness of low-frequency circulation patterns derived from EOF and rotated EOF analyses. *J. Climate,* **8,** 1709–1713.

Craddock, J. M., and C. R. Flood, 1969: Eigenvectors for representing the 500 mb geopotential surface over the Northern Hemisphere. *Quart. J. Roy. Meteor. Soc.,* **95,** 576–593.

Farrara, J. D., M. Ghil, C. R. Mechoso, and K. C. Mo, 1989: Empirical orthogonal functions and multiple flow regimes in the Southern Hemisphere winter. *J. Atmos. Sci.,* **46,** 3219–3223.

Ghil, M., and K. Mo, 1991: Instraseasonal oscillations in the global atmosphere. Part II: Southern Hemisphere. *J. Atmos. Sci.,* **48,** 780–790.

Hamilton, K., 1983: Aspects of wave behavior in the mid- and upper-troposphere of the Southern Hemisphere. *Atmos.–Ocean,* **21,** 40–54.

Horel, J. D., 1981: A rotated principal component analysis of the interannual variability of the Northern Hemisphere 500 mb height field. *Mon. Wea. Rev.,* **109,** 2080–2092.

Hoskins, B. J., and D. J. Karoly, 1981: The steady linear response of a spherical atmosphere to thermal and orographic forcing. *J. Atmos. Sci.,* **38,** 1179–1196.

——, H. H. Hsu, I. N. James, M. Masutani, P. D. Sardeshmuk, and G. H. White, 1989: Diagnostics of the global atmospheric circulation based on ECMWF analyses 1979–1989. WCRP 27, WMO/TD No. 326, WMO, Geneva, Switzerland, 217 pp.

Hsu, H., and J. M. Wallace, 1985: Vertical structure of wintertime teleconnection patterns. *J. Atmos. Sci.,* **42,** 1693–1710.

Hurrell, J., H. van Loon, and D. J. Shea, 1998: The mean state of the troposphere. *Meteorology of the Southern Hemisphere, Meteor. Monogr.,* No. 49, Amer. Meteor. Soc., 1–46.

Kalnay, E., and Coauthors, 1996: The NCEP/NCAR 40-year Reanalysis Project. *Bull. Amer. Meteor. Soc.,* **77,** 437–471.

Karoly, D. J., 1989: Southern Hemisphere circulation features associated with El Niño–Southern Oscillation events. *J. Climate,* **2,** 1239–1252.

——, 1990: The role of transient eddies in low-frequency zonal variations of the Southern Hemisphere circulation. *Tellus,* **42A,** 41–50.

Kidson, J. W., 1988a: Indices of the Southern Hemisphere zonal wind. *J. Climate,* **1,** 183–194.

——, 1988b: Interannual variations in the Southern Hemisphere circulation. *J. Climate,* **1,** 1177–1198.

——, 1991: Intraseasonal variations in the Southern Hemisphere circulation. *J. Climate,* **4,** 939–953.

——, and M. R. Sinclair, 1995: The influence of persistent anomalies on Southern Hemisphere storm tracks. *J. Climate,* **8,** 1938–1950.

Kiladis, G. N., and K. M. Weickmann, 1992a: Circulation anomalies associated with tropical convection during northern winter. *Mon. Wea. Rev.,* **120,** 1900–1923.

——, and ——, 1992b: Extratropical forcing of tropical Pacific convection during northern winter. *Mon. Wea. Rev.,* **120,** 1924–1938.

——, and ——, 1997: Horizontal structure and seasonality of large-scale circulations associated with submonthly tropical convection. *Mon. Wea. Rev.,* **125,** 1997–2013.

——, and K. C. Mo, 1998: Interannual and intraseasonal variability in the Southern Hemisphere. *Meteorology of the Southern Hemisphere, Meteor. Monogr.,* No. 49, Amer. Meteor. Soc., 307–336.

Kousky, V. E., and G. D. Bell, 1992: *Atlas of Southern Hemisphere 500 mb Teleconnection Patterns Derived from National Meteorological Center Analyses.* NOAA, NOAA Atlas No. 9, Dept. of Commerce, Camp Springs, MD, 90 pp.

Lau, K.-M., P.-J. Sheu, and I.-S. Kang, 1994: Multiscale low-frequency circulation modes in the global atmosphere. *J. Atmos. Sci.,* **51,** 1169–1193.

Madden, R., and P. Julian, 1994: Observations of the 40–50 day tropical oscillation—A review. *Mon. Wea. Rev.,* **122,** 814–837.

Mechoso, C. R., J. D. Farrara, and M. Ghil, 1991: Intraseasonal variability of the winter circulation in the Southern Hemisphere atmosphere. *J. Atmos. Sci.,* **48,** 1387–1404.

Mo, K. C., 1986: Quasi-stationary states in the Southern Hemisphere. *Mon. Wea. Rev.,* **114,** 808–823.

——, and H. van Loon, 1984: Some aspects of the interannual variation of mean monthly sea level pressure on the Southern Hemisphere. *J. Geophys. Res.,* **89** (D6), 9541–9546.

——, and G. H. White, 1985: Teleconnections in the Southern Hemisphere. *Mon. Wea. Rev.,* **113,** 22–37.

——, and M. Ghil, 1987: Statistics and dynamics of persistent anomalies. *J. Atmos. Sci.,* **44,** 877–901.

——, and R. W. Higgins, 1997: Planetary waves in the Southern Hemisphere and linkages to the tropics. Harry van Loon Symposium, Studies in Climate, Part II. NCAR Tech. Note TN-433+Proc., 290 pp.

——, and ——, 1998: The Pacific–South American modes and tropical convection during the Southern Hemisphere winter. *Mon. Wea. Rev.,* **126,** 1581–1596.

Newell, R. E., J. W. Kidson, D. G. Vincent, and G. J. Boer, 1972: *The General Circulation of the Tropical Atmosphere and Interactions with Extratropical Latitudes.* Vol. 1. The MIT Press, 258 pp.

North, G. R., T. L. Bell, R. F. Cahalan, and F. J. Moeng, 1982: Sampling errors in the estimation of empirical orthogonal functions. *Mon. Wea. Rev.,* **110,** 699–706.

O'Lenic, E. A., and R. E. Livezey, 1988: Practical considerations in the use of rotated principal component analysis (RPCA) in diagnostic studies of upper air heights. *Mon. Wea. Rev.,* **116,** 1682–1689.

Rasmusson, E. M., and K. Mo, 1993: Linkages between 200-mb

tropical and extratropical circulation anomalies during the 1986–1989 ENSO cycle. *J. Climate,* **6,** 595–616.

Renwick, J. A., R. J. Hurst, and J. W. Kidson, 1998: Climatic influences on the recruitment of Southern Gemfish (*Rexea Solandri, Gempylidae*) in New Zealand waters. *Int. J. Climatol.,* **18,** 1655–1667.

Richman, M. B., 1986: Rotation of principal components. *Int. J. Climatol.,* **6,** 293–335.

Rogers, J. C., and H. van Loon, 1982: Spatial variability of sea level pressure and 500 mb height anomalies over the Southern Hemisphere. *Mon. Wea. Rev.,* **110,** 1375–1392.

Salby, M. L., 1982: A ubiquitous wavenumber 5 anomaly in the Southern Hemisphere during FGGE. *Mon. Wea. Rev.,* **110,** 1712–1720.

Swanson, G. S., and K. E. Trenberth, 1981: Interannual variability in the Southern Hemisphere troposphere. *Mon. Wea. Rev.,* **109,** 1890–1897.

Trenberth, K. E., 1981: Observed Southern Hemisphere eddy statistics at 500 mb: Frequency and spatial dependence. *J. Atmos. Sci.,* **38,** 2585–2605.

——, 1991: Storm tracks in the Southern Hemisphere. *J. Atmos. Sci.,* **48,** 2159–2178.

——, and J. W. Hurrell, 1994: Decadal atmosphere–ocean variations in the Pacific. *Climate Dyn.,* **9,** 303–319.

——, G. W. Branstator, D. Karoly, A. Kumar, N.-C. Lau, and C. Ropelewski, 1998: Progress during TOGA in understanding and modeling global teleconnections associated with tropical sea surface temperatures. *J. Geophys. Res.,* **103** (C7), 14 291–14 324.

van Loon, H., J. W. Kidson, and A. B. Mullan, 1993: Decadal variation of the annual cycle in the Australian dataset. *J. Climate,* **6,** 1227–1231.

Wallace, J. M., and D. S. Gutzler, 1981: Teleconnections in the geopotential height field during the Northern Hemisphere winter. *Mon. Wea. Rev.,* **109,** 784–812.

White, W. B., and R. G. Peterson, 1996: An Antarctic circumpolar wave in surface pressure, wind, temperature and sea-ice extent. *Nature,* **380,** 699–702.

Yanai, M., and T. Tomita, 1998: Seasonal and interannual variability of atmospheric heat sources and moisture sinks as determined from NCEP–NCAR Reanalysis. *J. Climate,* **11,** 463–482.